ORIGINAL PAPER

A potential stress indicator for failure prediction of laboratory-scale rock samples

Lei Xue

Abstract Based on the two-dimensional renormalization group model, which can consider the stress transfer mechanism, in the present paper, the theoretical quantitative correlation between the threshold of the crack damage stress (σ_{cd}) and the uniaxial compressive strength (σ_{ucs}) was constructed. The results indicate that the normalized quantity σ_{cd}/σ_{ucs} decreases as the shape parameter m increases, and that it gradually tends towards a constant horizontal asymptote that is ~0.82. In addition, the experimental results of σ_{cd}/σ_{ucs} obtained in previous studies using different rock types were analyzed. From this analysis, it was found that the overall average and the standard deviation of σ_{cd}/σ_{ucs} for low-porosity rock samples is ~0.80 (±0.10), which would appear to be approximately consistent with the theoretical solution. This preliminary study indicates that the normalized quantity σ_{cd}/σ_{ucs} might be an intrinsic property of low-porosity rocks and thus could be regarded as a potential indicator for the failure prediction of laboratory-scale rock samples.

Keywords Failure prediction · Uniaxial compression test · Crack damage stress threshold · Renormalization group theory

Introduction

Generally, rock samples subjected to a uniaxial compression will manifest the typical mechanical responses shown in Fig. 1a. Classic works indicate that the failure process can be subdivided into five stages: (1) crack closure, (2) elastic deformation, (3) crack initiation and stable crack growth, (4) Crack damage and unstable crack growth, and (5) failure and post-peak behavior (Bieniawski 1967a, b; Brace et al. 1966; Lajtai and Lajtai 1974; Martin 1993; Xue et al. 2013). For a clearer presentation, the post-peak region is not depicted in Fig. 1a. There exist three stress thresholds prior to failure, i.e., the crack closure stress σ_{cc}, crack initiation stress σ_{ci}, and crack damage stress σ_{cd}. There is no doubt that if we could construct a quantitative relationship between the uniaxial compressive strength σ_{ucs} and any one of these three stress thresholds, the failure of rock samples could be predicted in advance.

It is well accepted that the macroscopic failure process of laboratory-scale rock samples is usually accompanied by accumulated micro-structural damage. In most cases, the cracks appear to be completely random in the beginning. However, as the applied load increases, additional cracks will develop and coalesce around the potential macroscopic fracture plane. When the rock sample can no longer bear the external load, ruptures may eventually occur. Numerous studies have indicated that as the stress magnitude gradually approaches the stress threshold σ_{cd}, crack propagation and interaction appear unstable and crack growth will not be terminated, even if the stress remains constant at σ_{cd} (Bieniawski 1967a, b; Brace et al. 1966; Eberhardt et al. 1997, 1998, 1999; Lajtai and Lajtai 1974; Martin and Chandler 1994). Conversely, when the external load is less than σ_{cd}, crack growth is stable. Furthermore, it has also been found that when the external load approaches the stress threshold σ_{cd}, some physical properties, such as acoustic emissions, permeability, wave velocity, and resistivity, generate significant responses (Chen and Lin 2004; Schulze et al. 2001; Souley et al. 2001; Sun et al. 2014).

It appears that the stress threshold σ_{cd} is a very special threshold. Therefore, we will attempt to establish a theoretical quantitative correlation between the crack damage stress threshold and uniaxial compressive strength. From Fig. 1b, it appears that rock samples usually suffer a phase transition

L. Xue (✉)
Key Laboratory of Shale Gas and Geoengineering, Institute of Geology and Geophysics, Chinese Academy of Sciences, Beijing 100029, China
e-mail: xuelei@mail.iggcas.ac.cn

Fig. 1 Illustration of phase transition of a system. **a** Typical stress–strain diagram showing different stages of crack development under uniaxial compression test. **b** The bifurcation evolution process of the renormalization group theory
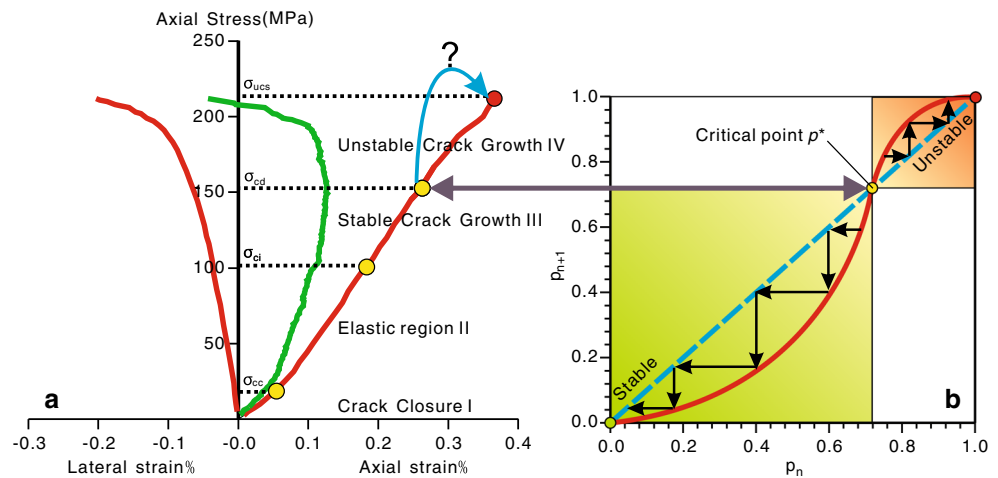
from a stable to unstable state at σ_{cd}, which is equivalent to the critical point in renormalization group (RG) theory. The so-called critical point is a term describing a singular point at which different phases or states coexist. In the field of geology and geophysics, numerous studies have reported on the phase transition of a system (Abdusalam 2001; Allegre et al. 1982; Borri-Brunetto et al. 2004; Carpinteri et al. 2001, 2002, 2012; Chen et al. 2002; Hansen et al. 1997; Iwashita and Nakanishi 2005; Madden 1983; Matsuba 2002; Meng et al. 2009; Saleur et al. 1996; Smalley et al. 1985). Therefore, the RG method is introduced in the present study to reveal the theoretical quantitative correlation between σ_{cd} and σ_{ucs}.

The structure of the present study is as follows. In second section, a detailed mathematical derivation of the theoretical solution of σ_{cd}/σ_{ucs} is described based on RG theory. Experimental findings and the discussion are presented in the third section. Finally, concluding remarks are presented in the fourth section.

Theoretical study of the relationship between the crack damage stress threshold and uniaxial compressive strength

The model of two-dimensional RG theory

It is well accepted that as the applied load gradually increases, cracks will develop and coalesce around the potential macroscopic fracture plane. Essentially, only when the crack density of the potential macroscopic fracture plane approaches a certain level will macroscopic fracture occurs. Therefore, the forming process of the macroscopic fracture plane is simplified and considered as a two-dimensional fracture process in the present work, and two-dimensional RG theory is introduced to describe the failure process of the rock samples (see Fig. 2). Thus, the macroscopic fracture plane can be renormalized into

many cells and different order blocks. Here, only the first three order blocks are shown. For example, the first-order block comprises four cells, while the second-order block consists of four first-order blocks. Similarly, the third-order block is composed of four second-order blocks. In fact, the same combination can be continued to an infinite scale. Furthermore, there exist five possible states for each of the different order blocks, i.e., B4U0, B3U1, B2U2, B1U3, and B0U4 (see Fig. 2d). The uppercase letter "B" denotes that the cells or blocks have been broken (colored box), which is followed by the digit corresponding to the number of broken cells or blocks. The uppercase letter "U" means that the cells or blocks have not been broken (white box), and the following digit corresponds to the number of unbroken cells or blocks. The corresponding probabilities of the five possible states are listed in column B of Table 1, where p_1 means the broken probability of each cell.

Methodology of two-dimensional RG theory

As suggested by Smalley et al. (1985), it is assumed that the strength of each individual cell is σ_{cell}, which obeys a Weibull distribution and depends on the number of microcracks in the cells. When an external load is applied to a rock sample, it is assumed that each cell of the rock will be subjected to a corresponding local stress. When the strength of the cell σ_{cell} is less than its local stress, the cell will fail, and its broken probability is p_α, which can be expressed as follows:

$$p_\alpha = p(\sigma_{cell} < \alpha\sigma) = 1 - \exp\left[-\left(\alpha\frac{\sigma}{\sigma_0}\right)^m\right], \quad (1)$$

where α is a coefficient, σ_0 is a reference strength of the cell, and m is a shape parameter that can be used to evaluate the discreteness of material strength. As suggested by Tang et al.

Fig. 2 Illustration of the two-dimensional RG model of macroscopic fracture plane. **a** Rock sample with two macroscopic fracture planes after failure under a uniaxial compression test. **b** Sketch showing two macroscopic fracture planes. **c** The two-dimensional RG model. **d** The five possible states for each block
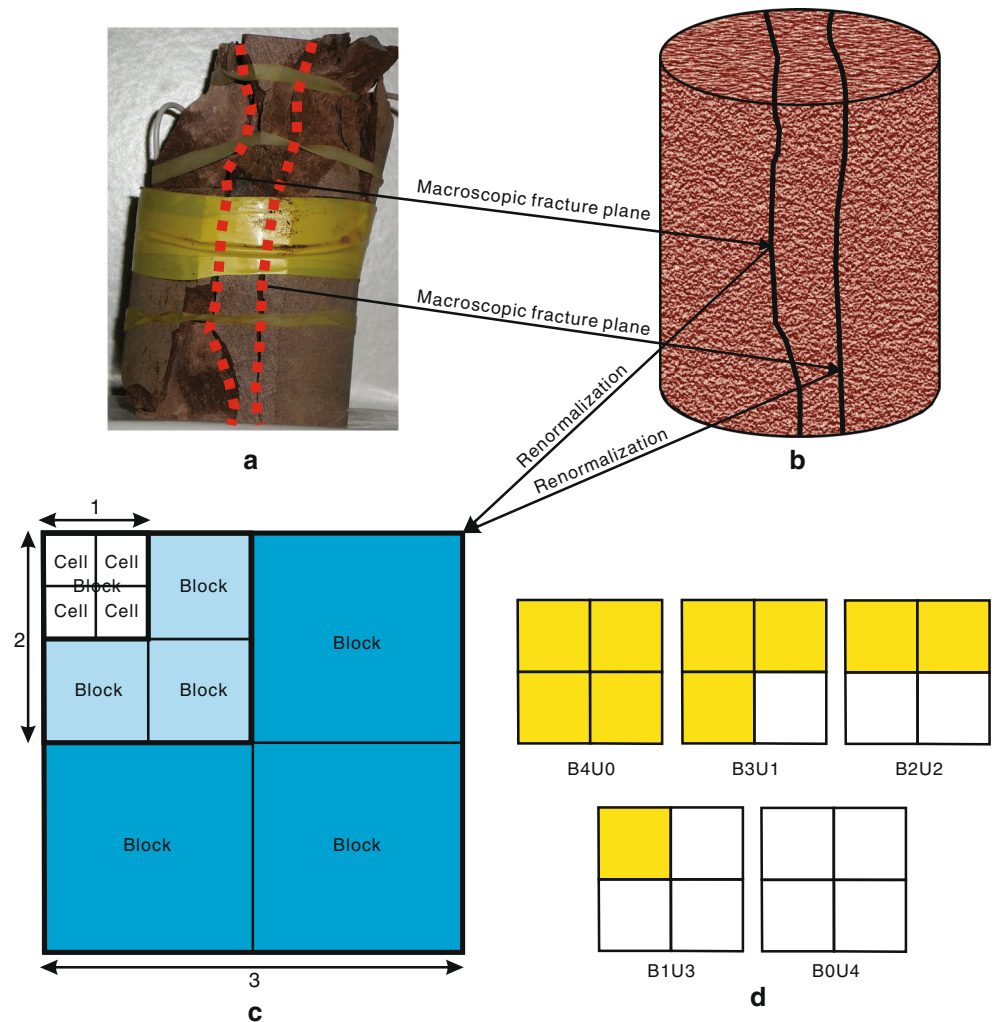
(2000) and Wong et al. (2006), the larger the shape parameter m, the more homogeneous the material. When α is equal to 1, namely

$$p_1 = p(\sigma_{cell} < \sigma) = 1 - \exp\left[-\left(\frac{\sigma}{\sigma_0}\right)^m\right]. \qquad (2)$$

By substituting Eq. (2) into Eq. (1), the following expression can be obtained:

$$p_\alpha = 1 - (1 - p_1)^{\alpha^m}. \qquad (3)$$

Table 1 Various probabilities for cells or blocks

Column A Block state	Column B The corresponding probability of block neglecting stress transfer	Column C The conditional failure probability of the unbroken cell or block due to stress transfer	Column D The overall failure probability of block considering stress transfer
B4U0	$C_4^4 p_1^4 (1-p_1)^0$	/	$D=B$
B3U1	$C_4^3 p_1^3 (1-p_1)^1$	$p_{4,1}$	$D=B \times C$
B2U2	$C_4^2 p_1^2 (1-p_1)^2$	$p_{2,1}^2 + C_2^1 p_{2,1}(1-p_{2,1})p_{4,2}$	$D=B \times C$
B1U3	$C_4^1 p_1^1 (1-p_1)^3$	$p_{4/3,1}^3 + C_3^2 p_{4/3,1}^2 \left(1-p_{4/3,1}\right)p_{4,4/3}$ $+ C_3^1 p_{4/3,1}\left(1-p_{4/3,1}\right)^2$ $\left[p_{2,4/3}^2 + C_2^1 p_{2,4/3}\left(1-p_{2,4/3}\right)p_{4,2}\right]$	$D=B \times C$
B0U4	$C_4^0 p_1^0 (1-p_1)^4$	/	$D=0$

It is worth noting that the broken cells will inevitably affect neighboring unbroken cells owing to the stress transfer. To evaluate the influence of the broken cells on their neighboring unbroken cells, a conditional probability $p_{m,n}$ is introduced, which can be expressed as follows:

$$p_{m,n} = \frac{p(n\sigma < \sigma_{cell} < m\sigma)}{p(\sigma_{cell} > n\sigma)} = \frac{p_m - p_n}{1 - p_n}, \tag{4}$$

where p_m and p_n can be calculated using Eq. (3). Essentially, the conditional probability $p_{m,n}$ is a probability that an unbroken cell with local stress $n\sigma$ will fail when subjected to an additional stress $(m-n)\sigma$ from a broken cell. At that moment, the overall local stress of the unbroken cell will increase to $m\sigma$. The conditional probabilities and overall broken probabilities of the five possible states are listed in columns C and D of Table 1, respectively.

Furthermore, some assumptions were made in this paper, as suggested in Smalley et al. (1985), namely:

(1) A $r+1^{\text{-th}}$ order block will not be regarded as a broken state unless all the $r^{\text{-th}}$ order blocks that compose this $r+1^{\text{-th}}$ order block are broken.
(2) The stress from a $r^{\text{-th}}$ order block, which belongs to a $r+1^{\text{-th}}$ order block, will be transferred uniformly to other $r^{\text{-th}}$ order blocks that belong to the same $r+1^{\text{-th}}$ order block.

Taking the first-order block with four cells as an example, its overall failure probability $p_1^{(2)}$ can be expressed as follows:

$$p_1^{(2)} = p_{b_4 u_0} + p_{b_3 u_1} + p_{b_2 u_2} + p_{b_1 u_3}, \tag{5}$$

where $p_{b_4 u_0}, p_{b_3 u_1}, p_{b_2 u_2}$, and $p_{b_1 u_3}$ are the overall failure probabilities of the different states of a cell, which can be obtained as shown in column D of Table 1.

Expanding Eq. (5) gives the following:

$$p_1^{(2)} = p_1^4 + C_4^3 p_1^3 (1-p_1) p_{4,1} + C_4^2 p_1^2 (1-p_1)^2 \left[p_{2,1}^2 + C_2^1 p_{2,1}(1-p_{2,1}) p_{4,2} \right]$$
$$+ C_4^1 p_1 (1-p_1)^3 \left\{ \begin{array}{l} p_{4/3,1}^3 + C_3^2 p_{4/3,1}^2 \left(1 - p_{4/3,1}\right) p_{4,4/3} + \\ C_3^1 p_{4/3,1} \left(1 - p_{4/3,1}\right)^2 \left[p_{2,4/3}^2 + C_2^1 p_{2,4/3}\left(1-p_{2,4/3}\right) p_{4,2} \right] \end{array} \right\}. \tag{6}$$

For higher-order blocks, Eq. (6) can also be extended to an iteration equation between $p_1^{(n+1)}$ and $p_1^{(n)}$, where

n is the order of the block. It can be expressed in the following form:

$$p_1^{(n+1)} = \left(p_1^{(n)}\right)^4 + C_4^3 \left(p_1^{(n)}\right)^3 \left(1 - p_1^{(n)}\right) p_{4,1}^{(n)} + C_4^2 \left(p_1^{(n)}\right)^2 \left(1 - p_1^{(n)}\right)^2$$
$$\left[\left(p_{2,1}^{(n)}\right)^2 + C_2^1 p_{2,1}^{(n)} \left(1 - p_{2,1}^{(n)}\right) p_{4,2}^{(n)} \right] + C_4^1 p_1^{(n)} \left(1 - p_1^{(n)}\right)^3$$
$$\left\{ \begin{array}{l} \left(p_{4/3,1}^{(n)}\right)^3 + C_3^2 \left(p_{4/3,1}^{(n)}\right)^2 \left(1 - p_{4/3,1}^{(n)}\right) p_{4,4/3}^{(n)} \\ + C_3^1 p_{4/3,1}^{(n)} \left(1 - p_{4/3,1}^{(n)}\right)^2 \left[\left(p_{2,4/3}^{(n)}\right)^2 + C_2^1 p_{2,4/3}^{(n)} \left(1 - p_{2,4/3}^{(n)}\right) p_{4,2}^{(n)} \right] \end{array} \right\}. \tag{7}$$

Based on Eq. (7), a iteration dependent relationship between $p_1^{(n+1)}$ and $p_1^{(n)}$ is obtained, which is shown in Fig. 3. It can be seen that there are three points where $p_1^{(n+1)}$ is equal to $p_1^{(n)}$ for each shape parameter m. Among the three points, 0 and 1 mean completely stable and completely unstable states, respectively, while the critical point p^* is a phase transition point, i.e., unstable fixed points, where the state changes from stable to unstable. It appears that the critical point p^* is equivalent to the concept of the stress threshold σ_{cd}.

Theoretical relationship between σ_{cd} and σ_{ucs}

The broken probability of a cell can also be written as (Qin et al. 2006)follows:

$$p = 1 - \exp\left[-\left(\frac{\varepsilon}{\varepsilon_0}\right)^m \right], \tag{8}$$

where ε_0 is a reference strain of the cell.

Then, by substituting p^* into Eq. (8),

$$\frac{\varepsilon_{cd}}{\varepsilon_0} = \left[-\ln\left(1 - p^*\right) \right]^{\frac{1}{m}}, \tag{9}$$

where ε_{cd} is the strain of the rock sample at σ_{cd}.

Furthermore, numerous studies have been performed to investigate the mechanical responses of rock samples (Chen et al. 2006; Li et al. 2012). Based on the statistics damage theory and Hooke's law, Chen et al. (2006) derived a constitutive formula as follows:

$$\sigma = E\varepsilon e^{-\left(\frac{\varepsilon}{\varepsilon_0}\right)^m}, \tag{10}$$

which could be used to describe the stress–strain curves of uniaxial compression tests.

It is well known that the first order derivative of Eq. (10) is equal to zero at the peak strength, i.e.
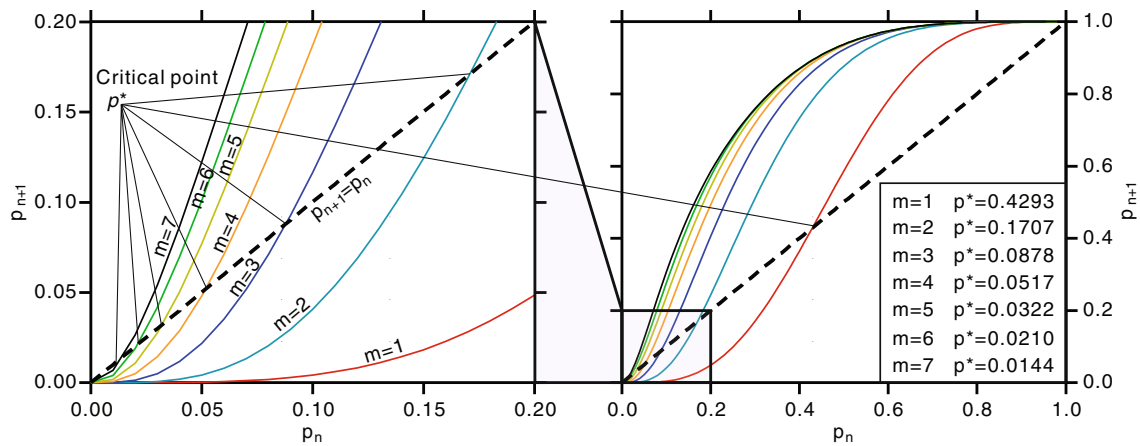
Fig. 3 Relationship between P_{n+1} and P_n and the illustration of critical point $p*$ for the two-dimensional RG model

$$\frac{\partial \sigma}{\partial \varepsilon} = E e^{-\left(\frac{\varepsilon}{\varepsilon_0}\right)^m} \left[1 - m(\varepsilon/\varepsilon_0)^m\right] = 0. \tag{11}$$

Rearranging Eq. (11) gives

$$\frac{\varepsilon_{ucs}}{\varepsilon_0} = \left(\frac{1}{m}\right)^{m^{-1}}, \tag{12}$$

where ε_{ucs} is the strain of the rock sample at the peak strength.

Then, calculating the ratio of Eq. (9) and Eq. (12) gives

$$\frac{\varepsilon_{ucs}}{\varepsilon_{cd}} = \left[-m\ln\left(1 - p^*\right)\right]^{-\left(\frac{1}{m}\right)}. \tag{13}$$

Substitution of Eq. (9) into Eq. (10) yields

$$\sigma_{cd} = E\varepsilon_{cd}\left(1 - p^*\right). \tag{14}$$

Substitution of Eq. (12) into Eq. (10) yields

$$\sigma_{ucs} = E\varepsilon_{ucs} e^{-(1 \; m)}. \tag{15}$$

The ratio of Eq. (14) to Eq. (15) is

$$\frac{\sigma_{cd}}{\sigma_{ucs}} = \frac{\varepsilon_{cd}}{\varepsilon_{ucs}}\left(1 - p^*\right) e^{\frac{1}{m}}. \tag{16}$$

Then, substituting Eq. (13) into Eq. (16) gives

$$\frac{\sigma_{cd}}{\sigma_{ucs}} = \left[-m\ln\left(1 - p^*\right)\right]^{\frac{1}{m}}\left(1 - p^*\right) e^{\frac{1}{m}}. \tag{17}$$

Thus, the theoretical quantitative relationship between the crack damage stress threshold and the peak strength is eventually established. It is found that $p*$ and the ratio of σ_{cd}/σ_{ucs} gradually decreases as the shape parameter m increases and the ratio of σ_{cd}/σ_{ucs} gradually tends towards a constant horizontal asymptote that is approximately 0.82 (see Table 2).

Experimental findings and discussion

Experimental findings

Many previous studies have investigated the stress threshold σ_{cd} or ratio of σ_{cd}/σ_{ucs} for different rock types, such as igneous rocks [involving granite (Cai et al. 2004; Chang and Lee 2004; Diederichs et al. 2004; Eberhardt et al. 1997, 1998, 1999; Hidalgo and Nordlund 2013; Liang et al. 2012; Lin et al. 2009; Takarli et al. 2008), gabbro (Hidalgo and Nordlund 2013), diabase (Hidalgo and Nordlund 2013), diorite (Andersson et al. 2009; Chen et al. 2012; Hidalgo and Nordlund 2013), and norite (Hidalgo and Nordlund 2013)], metamorphic rocks [involving marble (Chang and Lee 2004; Huang et al. 2012), quartzite (Cai et al. 2004; Hidalgo and Nordlund 2013), and gneiss (Hidalgo and Nordlund 2013)], and sedimentary rocks [involving sandstone (Cai et al. 2004; Gatelier et al. 2002; Jiang et al. 2005; Xu et al. 2012), limestone (Eslami et al. 2012; Hidalgo and Nordlund 2013; Palchik and Hatzor 2002), dolomite (Cai et al. 2004; Hatzor et al. 1997; Palchik and Hatzor 2002), coal (Ranjith et al. 2010), clay shale (Amann et al. 2011), and rock salt (Liang et al. 2011)]. The data of σ_{cd} or σ_{cd}/σ_{ucs} in the above literature have been given directly in the form of tables or pictures, thus greatly aiding our study. Recently, Xue et al. (2013) analyzed 251 sets of test data on different rock types and found that the average values of σ_{cd}/σ_{ucs} for the low-porosity igneous,

Table 2 Chart of theoretical solution based on two-dimensional RG method

Shape parameter m	Critical probability p^*	Normalized quantity σ_{cd}/σ_{ucs}
1	0.4293	0.8701
2	0.1707(0.1707)	0.8366
3	0.0878	0.8286
4	0.0517	0.8266
5	0.0322	0.8231
6	0.0210	0.8204
7	0.0144	0.8200
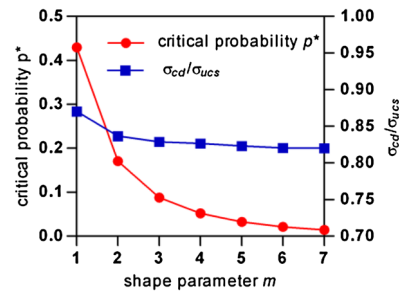
The results listed in parentheses are obtained by Smalley et al. (1985)

metamorphic, and sedimentary rocks were ~0.78 (±0.09), ~0.85 (±0.09), and ~0.78 (±0.11), respectively (see Fig. 4). Meanwhile, the corresponding overall average of σ_{cd}/σ_{ucs}

from the different rock types is equal to ~0.80 (±0.10), which appears approximately consistent with the theoretical solution.
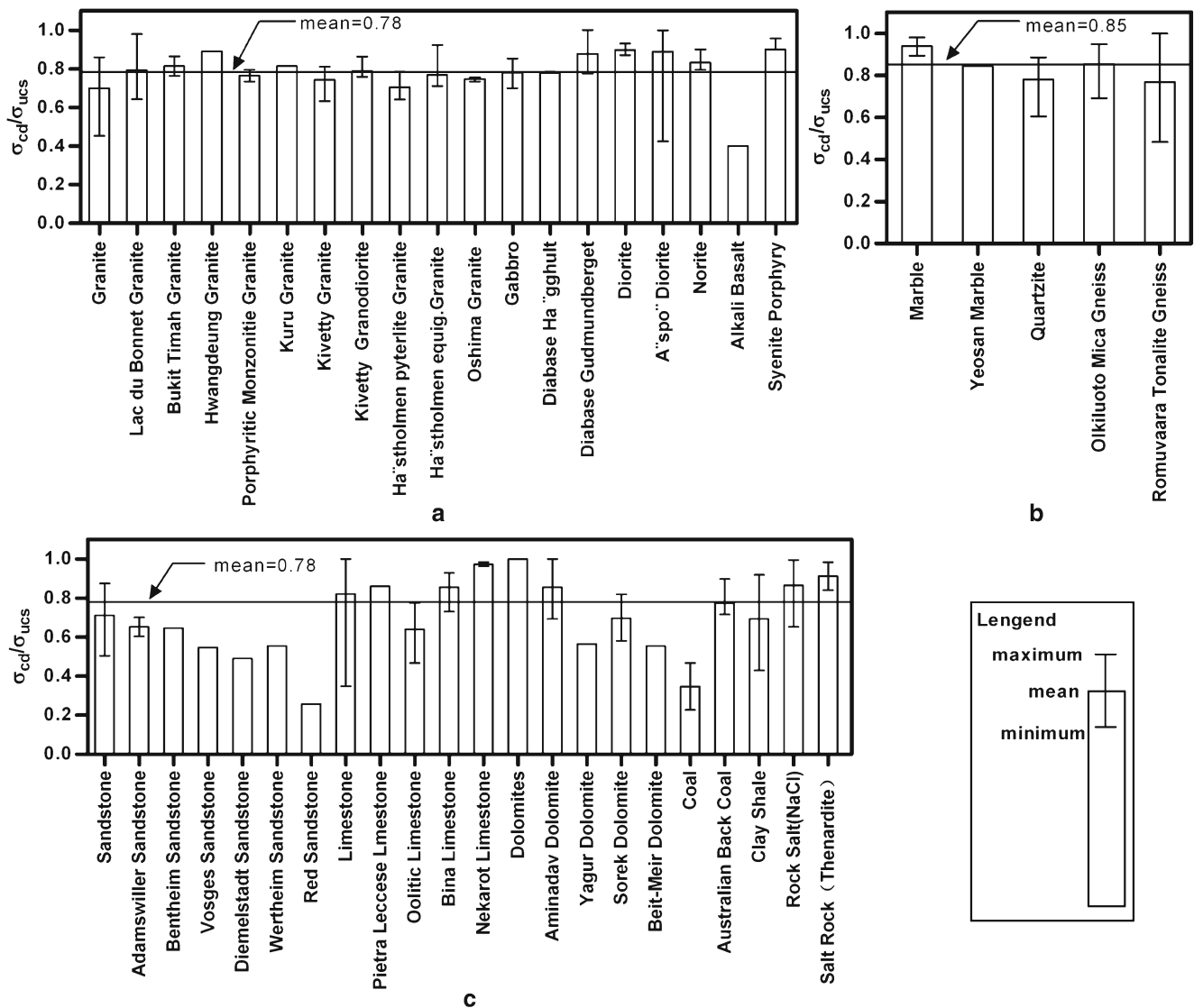

Fig. 4 Values of σ_{cd}/σ_{ucs} for different rock types: **a** igneous rock, **b** metamorphic rock, and **c** sedimentary rock (modified after Xue et al. (2013))

Fig. 5 Comparison between the theoretical solutions of σ_{cd}/σ_{ucs} and the experimental results of σ_{cd}/σ_{ucs} for low-porosity rocks. The seven *solid triangles* indicate the theoretical solutions of σ_{cd}/σ_{ucs} based on values of the shape parameter m from 1 to 7. The *horizontal solid line* is the overall average of the experimental results of σ_{cd}/σ_{ucs}, excluding data with values less than 0.6, as shown in Fig. 4
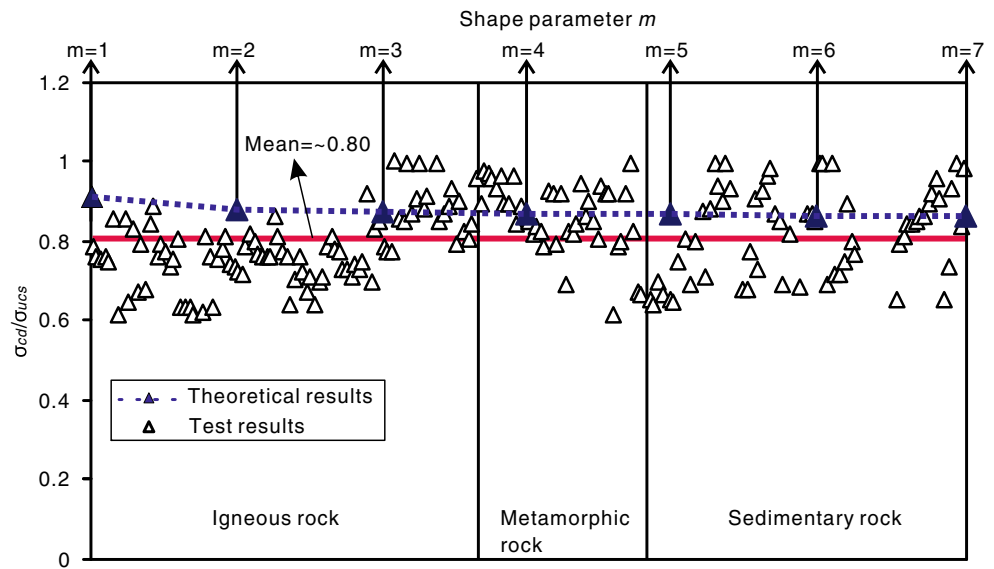
Discussion

Both the experimental results for low-porosity rock samples and the theoretical solutions (σ_{cd}/σ_{ucs}) are shown in Fig. 5. It is obvious that the distribution range of experimental results is wider than that of the RG solutions, which may be attributed to the following reasons:

Firstly, it has been found that the theoretical solution of σ_{cd}/σ_{ucs} varies with shape parameter m, which is used to evaluate the discreteness of the material's strength. However, Fig. RefID="Fig5">5 illustrates only the theoretical solutions based on values of parameter m from 1 to 7, and it is possible that the actual values of parameter m for the rock samples were outside this range. Therefore, it is necessary to conduct further studies to determine the actual shape parameter m of a rock sample in order that we can perform a strict comparison between the experimental results and theoretical solutions based on the same m value. This work is ongoing, in which the estimation of the shape parameter m relies on the method developed by Katz and Reches (2002).

Secondly, during the derivation process of the theoretical solution, it was assumed that the stress from broken blocks was transferred equally to the adjacent unbroken blocks, which may be an oversimplification of the real failure process. It may be more realistic that the stress be assigned according to the distance between the broken and unbroken blocks. In addition, other assumptions might also affect the theoretical solutions, for example, the choice of a two-dimensional RG model rather than a three-dimensional model. Therefore, we will attempt to conduct a more intensive theoretical study in future work.

In view of the above, Eq. (17) might be only an approximate theoretical relationship between σ_{cd} and σ_{ucs}. Nevertheless, it could be speculated that the ratio of σ_{cd}/σ_{ucs} might be an intrinsic property of low-porosity rocks, which could be considered as a reliable indicator for predicting the failure of laboratory-scale rock samples.

Conclusions

The present study investigated the relationship between the crack damage stress threshold and uniaxial compressive strength, based on experimental results and theoretical analysis. The following conclusions can be drawn:

(a) Based on uniaxial compression tests, it is determined that the overall average and standard deviation of σ_{cd}/σ_{ucs} of low-porosity rock samples is ~0.80 (±0.10).

(b) Based on the two-dimensional RG method, we eventually established the theoretical solution of σ_{cd}/σ_{ucs}. It was found that as the shape parameter m increases, the ratio σ_{cd}/σ_{ucs} gradually decreases and tends towards a horizontal asymptote that is almost consistent with the overall average of experiment results, i.e., ~0.80.

(c) Both the experimental results and theoretical solutions imply that there exists a certain relationship between σ_{cd} and σ_{ucs}. The normalized quantity, σ_{cd}/σ_{ucs}, might be an intrinsic property of low-porosity rocks, which could be regarded as a potential indicator for predicting the failure of laboratory-scale rock samples.

References

Abdusalam HA (2001) Renormalization group method and Julia sets. Chaos, Solitons Fractals 12(2):423–428. doi:10.1016/S0960-0779(00)00008-4

Allegre C, Le Mouel J, Provost A (1982) Scaling rules in rock fracture and possible implications for earthquake prediction. Nature 297:47–49. doi:10.1038/297047a0

Amann F, Button EA, Evans KF, Gischig VS, Blumel M (2011) Experimental study of the brittle behavior of clay shale in rapid unconfined compression. Rock Mech Rock Eng 44(4):415–430. doi:10.1007/s00603-011-0156-3

Andersson JC, Martin CD, Stille H (2009) The Äspö pillar stability experiment: part II—rock mass response to coupled excavation-induced and thermal-induced stresses. Int J Rock Mech Min 46(5):879–895. doi:10.1016/j.ijrmms.2009.03.002

Bieniawski ZT (1967a) Mechanism of brittle fracture of rock: part I—theory of the fracture process. Int J Rock Mech Min 4(4):395–406. doi:10.1016/0148-9062(67)90030-7

Bieniawski ZT (1967b) Mechanism of brittle fracture of rock: part II—experimental studies. Int J Rock Mech Min 4(4):407–423. doi:10.1016/0148-9062(67)90031-9

Borri-Brunetto M, Carpinteri A, Chiaia B (2004) The effect of scale and criticality in rock slope stability. Rock Mech Rock Eng 37(2):117–126. doi:10.1007/s00603-003-0004-1

Brace WF, Paulding BW, Scholz CH (1966) Dilatancy in the fracture of crystalline rocks. J Geophys Res 71(16):3939–3953. doi:10.1029/JZ071i016p03939

Cai M, Kaiser P, Tasaka Y, Maejima T, Morioka H, Minami M (2004) Generalized crack initiation and crack damage stress thresholds of brittle rock masses near underground excavations. Int J Rock Mech Min 41(5):833–847. doi:10.1016/j.ijrmms.2004.02.001

Carpinteri A, Chiaia B, Cornetti P (2001) Static–kinematic duality and the principle of virtual work in the mechanics of fractal media. Comput Method Appl Mech Eng 191(1):3–19. doi:10.1016/S0045-7825(01)00241-9

Carpinteri A, Chiaia B, Invernizzi S (2002) Applications of fractal geometry and renormalization group to the Italian seismic activity. Chaos, Solitons Fractals 14(6):917–928. doi:10.1016/S0960-0779(02)00081-4

Carpinteri A, Corrado M, Lacidogna G (2012) Three different approaches for damage domain characterization in disordered materials: fractal energy density, b-value statistics, renormalization group theory. Mech Mater 53:15–28. doi:10.1016/j.mechmat.2012.05.004

Chang SH, Lee CI (2004) Estimation of cracking and damage mechanisms in rock under triaxial compression by moment tensor analysis of acoustic emission. Int J Rock Mech Min 41(7):1069–1086. doi:10.1016/j.ijrmms.2004.04.006

Chen GY, Lin YM (2004) Stress–strain–electrical resistance effects and associated state equations for uniaxial rock compression. Int J Rock Mech Min 41(2):223–236. doi:10.1016/S1365-1609(03)00092-3

Chen Z, Tham L, Yeung M, Tsui Y, Lee P (2002) A study on the peak strength of brittle rocks. Rock Mech Rock Eng 35(4):255–270. doi:10.1007/s00603-002-0029-x

Chen ZH, Tham LG, Yeung MR, Xie H (2006) Confinement effects for damage and failure of brittle rocks. Int J Rock Mech Min 43(8):1262–1269. doi:10.1016/j.ijrmms.2006.03.015

Chen YF, Li DQ, Jiang QH, Zhou CB (2012) Micromechanical analysis of anisotropic damage and its influence on effective thermal conductivity in brittle rocks. Int J Rock Mech Min 50:102–116. doi:10.1016/j.ijrmms.2011.11.003

Diederichs MS, Kaiser PK, Eberhardt E (2004) Damage initiation and propagation in hard rock during tunnelling and the influence of near-face stress rotation. Int J Rock Mech Min 41(5):785–812. doi:10.1016/j.ijrmms.2004.02.003

Eberhardt E, Stead D, Stimpson B, Read R (1997) Changes in acoustic event properties with progressive fracture damage. Int J Rock Mech Min 34(3–4):71. e71–71. e12. doi:10.1016/S1365-1609(97)00062-2

Eberhardt E, Stead D, Stimpson B, Read R (1998) Identifying crack initiation and propagation thresholds in brittle rock. Can Geotech J 35(2):222–233

Eberhardt E, Stead D, Stimpson B (1999) Quantifying progressive pre-peak brittle fracture damage in rock during uniaxial compression. Int J Rock Mech Min 36(3):361–380. doi:10.1016/S0148-9062(99)00019-4

Eslami J, Hoxha D, Grgic D (2012) Estimation of the damage of a porous limestone using continuous wave velocity measurements during uniaxial creep tests. Mech Mater 49:51–65. doi:10.1016/j.mechmat.2012.02.003

Gatelier N, Pellet F, Loret B (2002) Mechanical damage of an anisotropic porous rock in cyclic triaxial tests. Int J Rock Mech Min 39(3):335–354. doi:10.1016/S1365-1609(02)00029-1

Hansen A, Roux SR, Aharony A, Feder J, Jøssang T, Hardy HH (1997) Real-space renormalization estimates for two-phase flow in porous media. Transport Porous Media 29(3):247–279. doi:10.1023/A:1006593820928

Hatzor YH, Zur A, Mimran Y (1997) Microstructure effects on microcracking and brittle failure of dolomites. Tectonophysics 281(3):141–161. doi:10.1016/S0040-1951(97)00073-5

Hidalgo KP, Nordlund E (2013) Comparison between stress and strain quantities of the failure–deformation process of Fennoscandian hard rocks using geological information. Rock Mech Rock Eng 46(1):41–51. doi:10.1007/s00603-012-0242-1

Huang D, Huang RQ, Zhang YX (2012) Experimental investigations on static loading rate effects on mechanical properties and energy mechanism of coarse crystal grain marble under uniaxial compression. China J Rock Mech Eng 31(2):245–255 (in Chinese)

Iwashita Y, Nakanishi I (2005) Scaling laws of earthquakes derived by renormalization group method. Chaos, Solitons Fractals 24(2):511–518. doi:10.1016/j.chaos.2004.08.002

Jiang YD, Xian XF, Xiong DG, Zhou FC (2005) Study on creep behaviour of sandstone and its mechanical models. Chin Journal Geotech Eng 27(12):1478–1481 (in Chinese)

Katz O, Reches Z (2002) Pre-failure damage, time-dependent creep and strength variations of a brittle granite. In: Proceedings, 5th international conference on analysis of discontinuous deformation, Ben-Gurion University, Balkema, Rotterdam

Lajtai EZ, Lajtai VN (1974) The evolution of brittle fracture in rocks. J Geol Soc Lond 130(1):1–16. doi:10.1144/gsjgs.130.1.0001

Li X, Cao WG, Su YH (2012) A statistical damage constitutive model for softening behavior of rocks. Eng Geol 143:1–17. doi:10.1016/j.enggeo.2012.05.005

Liang WG, Zhao YS, Xu SG, Dusseault MB (2011) Effect of strain rate on the mechanical properties of salt rock. Int J Rock Mech Min 48(1):161–167. doi:10.1016/j.ijrmms.2010.06.012

Liang CY, Li X, Wang SX, Li SD, He JM, Ma CF (2012) Experimental investigations on rate-dependent stress–strain characteristics and energy mechanism of rock under uniaixal compression. China J Rock Mech Eng 31(9):1830–1838 (in Chinese)

Lin QX, Liu YM, Tham LG, Tang CA, Lee PKK, Wang J (2009) Time-dependent strength degradation of granite. Int J Rock Mech Min 46(7):1103–1114. doi:10.1016/j.ijrmms.2009.07.005

Madden TR (1983) Microcrack connectivity in rocks: a renormalization group approach to the critical phenomena of conduction and failure in crystalline rocks. J Geophys Res: Solid Earth (1978–2012) 88(B1):585–592. doi:10.1029/JB088iB01p00585

Martin CD (1993) The strength of massive Lac du Bonnet granite around underground openings. University of Manitoba, Winnipeg

Martin CD, Chandler NA (1994) The progressive fracture of Lac du Bonnet granite. Int J Rock Mech Min Geomech Abstr 31(6):643–659. doi:10.1016/0148-9062(94)90005-1

Matsuba I (2002) Renormalization group approach to earthquake scaling. Chaos, Solitons Fractals 13(6):1281–1294. doi:10.1016/S0960-0779(01)00134-5

Meng XR, Gao ZN, Wang XQ (2009) Study on critical conditions for rock failure by means of group renormalization. J Coal Sci Eng (China) 15(1):50–54

Palchik V, Hatzor YH (2002) Crack damage stress as a composite function of porosity and elastic matrix stiffness in dolomites and limestones. Eng Geol 63(3):233–245. doi:10.1016/S0013-7952(01)00084-9

Qin SQ, Jiao JJ, Tang CA, Li ZG (2006) Instability leading to coal bumps and nonlinear evolutionary mechanisms for a coal-pillar-and-roof system. Int J Solids Struct 43(25–26):7407–7423. doi:10.1016/j.ijsolstr.2005.06.087

Ranjith PG, Jasinge D, Choi SK, Mehic M, Shannon B (2010) The effect of CO_2 saturation on mechanical properties of Australian black coal using acoustic emission. Fuel 89(8):2110–2117. doi:10.1016/j.fuel.2010.03.025

Saleur H, Sammis CG, Sornette D (1996) Renormalization group theory of earthquakes. Nonlinear Proc Geophys 3(2):102–109. doi:10.5194/npg-3-102-1996

Schulze O, Popp T, Kern H (2001) Development of damage and permeability in deforming rock salt. Eng Geol 61(2):163–180. doi:10.1016/S0013-7952(01)00051-5

Smalley RF, Turcotte DL, Solla SA (1985) A renormalization group approach to the stick-slip behavior of faults. J Geophys Res: Solid Earth (1978–2012) 90(B2):1894–1900. doi:10.1029/JB090iB02p01894

Souley M, Homand F, Pepa S, Hoxha D (2001) Damage-induced permeability changes in granite: a case example at the URL in Canada. Int J Rock Mech Min 38(2):297–310. doi:10.1016/S1365-1609(01)00002-8

Sun Q, Zhu S, Xue L (2014) Electrical resistivity variation in uniaxial rock compression. Arab J Geosci 1–12. doi:10.1007/s12517-014-1381-3

Takarli M, Prince W, Siddique R (2008) Damage in granite under heating/cooling cycles and water freeze-thaw condition. Int J Rock Mech Min 45(7):1164–1175. doi:10.1016/j.ijrmms.2008.01.002

Tang C, Liu H, Lee P, Tsui Y, Tham L (2000) Numerical studies of the influence of microstructure on rock failure in uniaxial compression—part I: effect of heterogeneity. Int J Rock Mech Min 37(4):555–569. doi:10.1016/S1365-1609(99)00121-5

Wong TF, Wong RH, Chau K, Tang C (2006) Microcrack statistics, Weibull distribution and micromechanical modeling of compressive failure in rock. Mech Mater 38(7):664–681. doi:10.1016/j.mechmat.2005.12.002

Xu NC, Yang XY, Qin J (2012) Relationship between rock's bulk strain and long-term strength under uniaxial compression. J Liaoning Tech Univ 31(3):358–361 (in Chinese)

Xue L, Qin SQ, Sun Q, Wang YY, Lee LM, Li WC (2013) A study on crack damage stress thresholds of different rock types based on uniaxial compression tests. Rock Mech Rock Eng 1–13. doi:10.1007/s00603-013-0479-3